Communication

Investigations on Microstructure and Mechanical Properties of AZ91 Alloy Processed by Single Pass Rolling with Varied Rolling Reductions

Yuhua Li [1], Qiong Xu [2,3,*], Aibin Ma [1,*], Jin Zhang [3], Yalong Shen [3], Jinghua Jiang [1], Yaqing Jiang [1] and Huan Liu [1]

1   College of Mechanics and Materials, Hohai University, Nanjing 211100, China
2   School of Materials and Chemical Engineering, Anhui Jianzhu University, Hefei 230601, China
3   School of Mechanical and Electrical Engineering, Suqian College, Suqian 223800, China
*   Correspondence: qxu2023@ahjzu.edu.cn (Q.X.); aibin-ma@hhu.edu.cn (A.M.); Tel.: +86-152-5185-6392 (Q.X.); +86-25-8378-7239 (A.M.); Fax: +86-0551-6382-8163 (Q.X.); +86-25-8378-6046 (A.M.)

Abstract: In this study, single pass rolling (SPR) with varied rolling reductions was conducted on pre-homogenized AZ91 alloys (H alloys) and ECAP-processed AZ91 alloys (HE alloys). The effects of rolling reduction on the microstructures and mechanical properties of HR alloys (pre-homogenized and rolled) and HER alloys (ECAP-processed and rolled) were investigated. The results showed that the HER alloys possessed much finer microstructures and superior mechanical properties than the HR alloys, which were significantly influenced by the rolling reduction. The microstructures of the HER alloys became bimodal, and the strength and elongation markedly improved with the increase in the rolling reduction. When the rolling reduction reached 70%, the HER alloys acquired a typical bimodal structure, contributing to their excellent comprehensive mechanical properties.

Keywords: metals and alloys; microstructure; single pass rolling (SPR); rolling reduction; mechanical properties

1. Introduction

Magnesium (Mg) alloys have excellent properties, such as low density, high specific strength, and good damping capacity [1,2]. Much attention has been paid to their applications in multiple areas, including automobiles, high-speed railways, aerospace, and electronics, where thin-walled components are often contained [3,4]. The development of Mg alloy sheets and/or plates with excellent mechanical properties plays a pivotal part in extending Mg alloys' applications.

Rolling is the most commonly used method of producing metal profiles and plates [5,6]. However, the plasticity of Mg alloys is poor due to their hexagonal close-packed (HCP) crystal structure. Mg alloy rolled sheets are traditionally fabricated through multi-pass rolling with small thickness reductions (5–10% at each pass) and intermediate high-temperature annealing [7,8]. This results in low economic and time efficiency when producing Mg alloy sheets. To overcome these problems, new rolling techniques such as differential speed rolling (DSR) [9,10], equal channel angular rolling (ECAR) [11,12], asymmetric rolling (AR) [13,14], and hard plate rolling (HPR) [15,16] have been developed. However, the application of newly developed methods to industrial production in many areas has not yet been advanced. Therefore, another significant consideration is to alter the hard-to-deform Mg alloys and improve their plasticity in advance, which would allow the advantages of conventional rolling to be fully utilized.

Severe plastic deformation (SPD) has been prevailing method used to produce ultrafine structures and improved mechanical properties in metallic materials [17–20]. Among the various SPD methods, material researchers have focused on equal channel angular pressing

(ECAP), as it can effectively produce bulk metallic materials with ultrafine grains, which are potentially suitable for practical applications [21–25]. It has been reported that ECAP is effective in improving the ductility of magnesium alloys, but its strength enhancement effect is not that ideal [26,27]. The ductility is usually improved in ECAP-processed Mg alloys, as a beneficial deformation texture is formed, while the yield strength enhancement is limited because of the easily activated basal slip caused by its special texture [26,27]. This indicates that it is necessary to further strengthen ECAP-processed Mg alloys. Lu et al. [28] obtained an ultrafine crystal structure in an Mg–Gd–Zn–Zr magnesium alloy with ECAP and improved its rolling formability and mechanical properties. Yuan et al. [29] applied ECAP and conventional cold rolling on a ZK60 Mg alloy and found that the specific deformation texture formed by ECAP favored the basal slip and tension twinning in the rolling that followed. Therefore, ECAP can be used as a preprocessing technique to improve the formability of Mg alloys as it facilitates further plastic deformation, and to achieve strength improvement in Mg alloys.

Mg-9Al-1Zn (AZ91) alloys have been extensively studied among the various Mg alloys because of their high strength, good machinability, and adequate corrosion resistance. In our previous study [30], the deformation properties of commercial AZ91 alloys were effectively improved by rotary-die equal channel angular pressing (RD-ECAP) processing. The RD-ECAP-processed AZ91 alloys could be subjected to high reduction rolling, with edge cracks largely eliminated and mechanical properties greatly improved. However, the effect of the varied rolling reduction on the rolling behavior of RD-ECAP-processed AZ91 alloys has not been studied. Therefore, single pass rolling (SPR) with varied rolling reduction was applied here, and the effects of rolling reduction on the microstructures and mechanical properties of the rolled AZ91 plates were discussed.

2. Materials and Methods

A commercial AZ91 cast ingot with a nominal chemical composition of 9.01-wt.% Al, 0.71-wt.% Zn, and 0.18-wt.% Mn (Yueyang Yuhua Metallurgical New Materials Co., Ltd., Yueyang, China) was used in this study. The chemical composition of the AZ91 alloy is presented in Table 1. A piece of upscaled rotary-die (RD) ECAP equipment (Wuxi Haofei Machinery Factory, Wuxi, Jiangsu, China) was used to prepare large-scale ECAP samples with a cross-section dimension of 50 mm × 50 mm and a length of 100 mm. A conventional two-roll mill device (Wuxi Jingcheng Machinery Co., Ltd., Wuxi, China) was used for the rolling process. The dimensions of each roller are Φ 240 mm × 400 mm. The ingot was cut into 50 mm × 50 mm × 100 mm cuboids, followed by a 24 h solution heat treatment at 420 °C and subsequent quenching in water (henceforth referred to as the H alloys). Then, the cuboids continually underwent 16 passes at 300 °C and a pressing speed of 2.5 mm/s through the RD-ECAP equipment, followed by rapid water cooling (henceforth referred to as the HE alloys). The H and HE alloys were used to produce plates parallel to the rectangular plane with thicknesses of 2.6, 3.3, 5.1, and 6.9 mm. The plates were heated to 400 °C and kept for 5 min, then rolled to ~2.0 mm by SPR with the two-roll mill device, which had been heated to 80 °C beforehand. The rolling reductions were calculated to be ~20%, ~40%, ~60%, and ~70%, respectively. The operation principle and details of the ECAP process and the rolling process can be found in our previous work [30,31]. The rolled H and HE alloys were named the HR alloys and HER alloys, respectively.

Table 1. Chemical composition of the AZ91 alloy used in this study.

Elements	Al	Zn	Mn	Cu	Si	Fe	Ni	Mg
wt.%	9.01	0.71	0.18	0.0026	0.0033	0.0026	0.0006	Remaining

The microstructures were examined by optical microscopy (OM, Olympus BX51M, Shinjuku, Tokyo, Japan) and field-emission scanning electron microscopy (SEM, Zeiss Sigma 300, Oberkochen, Germany). The samples prepared for OM and SEM observations were me-

chanically polished and were etched in acetic–picric solution. The grain maps were obtained by a field-emission scanning electron microscope equipped with an electron backscattered diffraction (SEM-EBSD, Hitachi S-3400 N, Hitachi, Chiyoda, Tokyo, Japan). Transmission electron microscopy (TEM) analysis was performed with an FEI Tecnai-G2 thermo-emission transmission electron microscope (FEI Tecnai G2 T20, Hillsboro, OR, USA).

Tensile tests were performed according to the ASTM E8 standard on a universal tensile testing machine (SHIMADZU AGS-X 20KN, Suzhou, China) at room temperature with a tensile speed of 0.5 mm/min. The gauge length and the width of the testing samples were 6 mm and 2 mm, respectively. Three samples were tested for each condition.

3. Results

Figure 1 presents the microstructures of the as-cast, H, and HR alloys. As shown in Figure 1a, a coarse dendrite structure was observed in the as-cast alloy where coarse β-$Mg_{17}Al_{12}$ second phases were embedded in the α-Mg. After heat treatment, the β-$Mg_{17}Al_{12}$ phases dissolved into the matrix, and large grains were generated because of the high-temperature homogenization, as shown in Figure 1b. After further rolling, the microstructures of the alloys remained coarse, as shown in Figure 1c–f. Twinning was observed in the HR alloys processed by SPR with varied rolling reductions; as the H alloys have a poor plasticity, deformation twinning was activated to accommodate the applied rolling deformation [32]. When the rolling reduction increased, narrow localized deformation bands were also observed, as presented in the SEM image inset in Figure 1f.
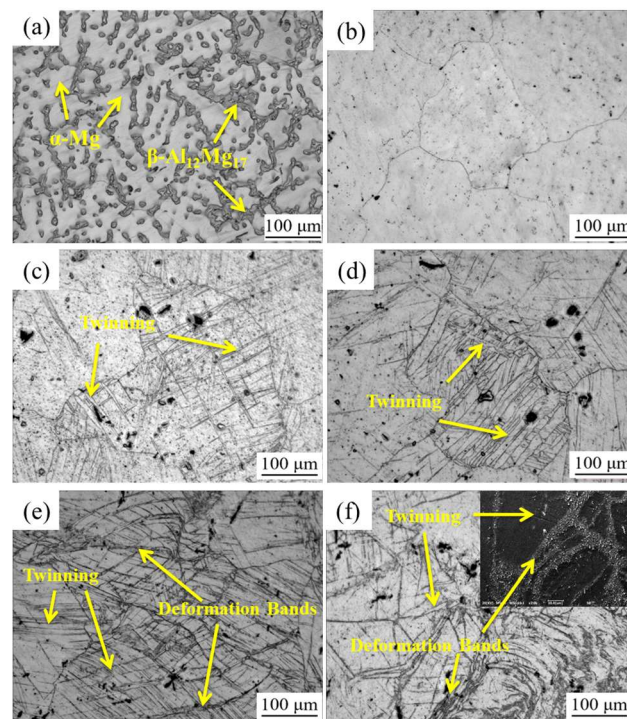

Figure 1. Microstructures of the (**a**) as-cast, (**b**) H, (**c**) 20%-HR, (**d**) 40%-HR, (**e**) 60%-HR, and (**f**) 70%-HR alloys.

Figure 2 shows the microstructures of the HE alloy, the heated HE alloy, and the HER alloys. The EBSD grain maps and grain-size statistics of the HER alloys are presented in Figure 3. As shown in Figure 2a, the HE alloy showed a homogenized fine structure containing small α-Mg grains and tiny β-$Mg_{17}Al_{12}$ particles. The average grain size is 3.39 μm, as displayed in the grain-size statistics inset in Figure 2a. After preheating, the grains grew up to tens of microns and the second phase dissolved into the matrix, as illustrated in Figure 2b,c. After further rolling, finer microstructures were formed in the

HER alloys as compared to those of the HR alloys. As shown in Figure 2d, the 20%-HER alloy possessed a homogenous grain structure that is very similar to that of the heated HE alloy. The grain size was normally distributed on the grain area distribution map, as presented in Figure 3a,b. As shown in Figure 2e, the microstructure of the 40%-HER alloy was similar to that of the 20% sample, and the grain size was approximately normally distributed, as presented in Figure 3c,d. When the rolling reduction increased to 60%, fine grains appeared, and the grains tended to be bimodal, as shown in Figures 2f and 3e,f. After the rolling reduction reached 70%, the bimodal characteristics of the distribution became more evident, as illustrated in Figures 2g and 3g,h. If classified by a critical grain size of 30 μm, the average grain size is 75.6 μm and 3.6 μm, for grains with grain size larger than 30 μm and smaller than 30 μm, respectively. The distribution was a typical bimodal distribution. The TEM and SEM micrographs presented in Figure 2h,i revealed that the fine grain region contained numerous nanoscale β-$Mg_{17}Al_{12}$ phases.

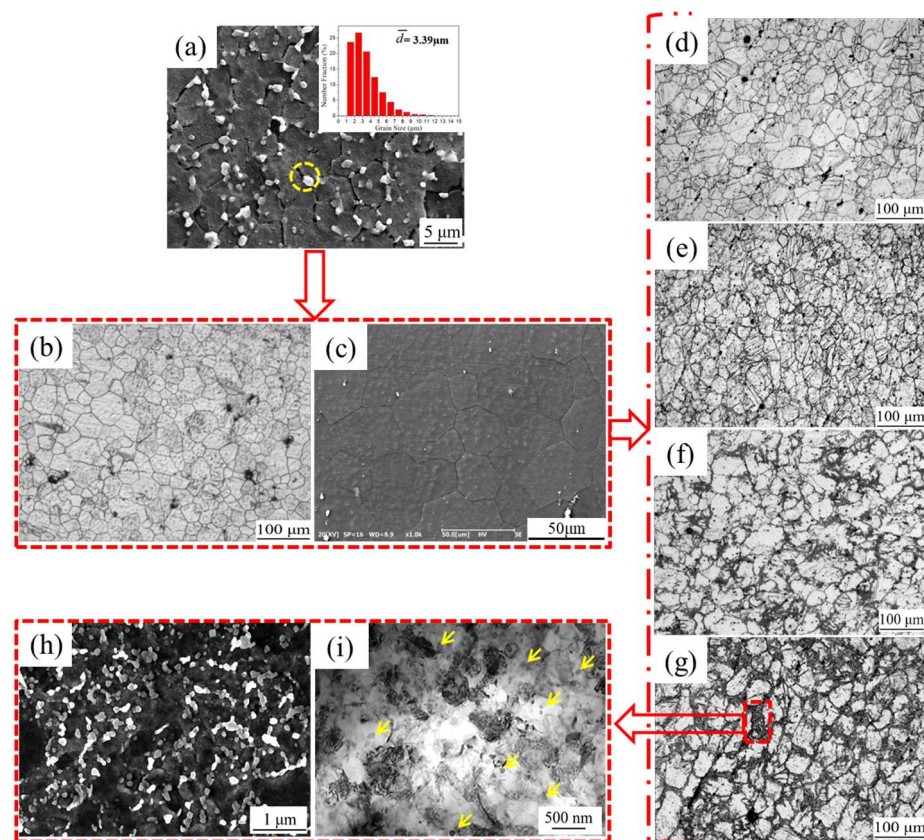**Figure 2.** Microstructures of the (**a**) HE alloy [30], (**b**,**c**) heated HE alloy, (**d**) 20%-HER alloy, (**e**) 40%-HER alloy, (**f**) 60%-HER alloy, and (**g**–**i**) 70%-HER alloy [30]; (**a**,**c**,**h**) SEM image, (**b**,**d**–**g**) optical microstructures, and (**i**) TEM image.

Figure 4a,b present the typical stress–strain curves of the H, HR, HE, and HER alloys. Their tensile properties are compared in Figure 4c,d. The H alloys exhibited poor mechanical properties, of which the ultimate tensile strength (UTS) was around 210 MPa. The HE alloy had a good trade-off of stress and strain, while the yield strength (YS) was still insufficient. After rolling, the stresses increased and the strains decreased in the HR and HER alloys as compared to those of the H and HE alloys, respectively. Despite this similarity, the HER alloys possessed superior comprehensive mechanical properties, of which the UTSs were over 350 MPa and the engineering strains were all above 10%. The HR alloys exhibited relatively poorer mechanical properties, of which the UTSs were under 330 MPa and the strains were less than 5%. The comprehensive mechanical properties of the HER alloys were significantly improved as the rolling reduction increased from 20% to

70%. At the rolling reduction of 70%, the HER alloy obtained the best comprehensive mechanical properties. This alloy yielded the highest ultimate strength and yield strength, at ~420 MPa and ~335 MPa, respectively, and simultaneously obtained the largest elongation, at ~19%. This was attributed to its typical bimodal structure, where fine grains provide grain boundary strengthening and enhanced strength, while coarse grains enable strain hardening and hence improve ductility [30,33].
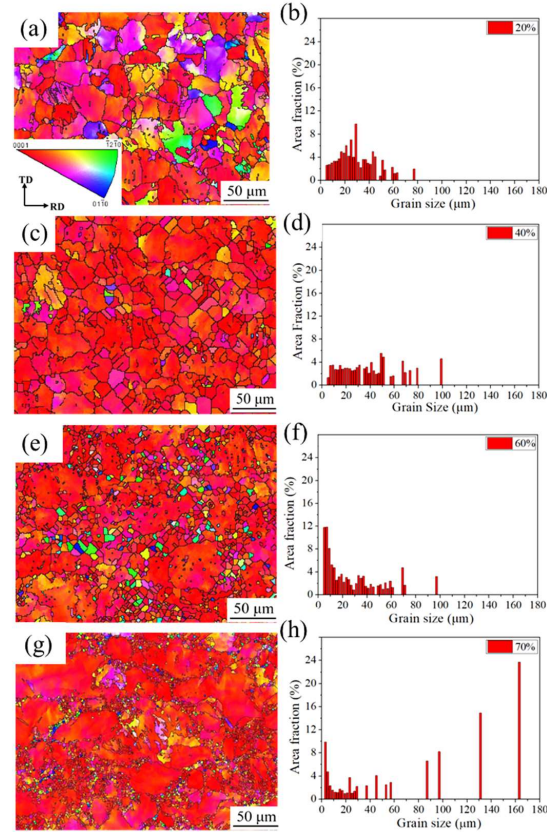

Figure 3. The (**a**,**c**,**e**,**g**) EBSD grain maps and (**b**,**d**,**f**,**h**) grain-size statistics of the HER alloys; (**a**,**b**) 20%-HER alloy, (**c**,**d**) 40%-HER alloy, (**e**,**f**) 60%-HER alloy, and (**g**,**h**) 70%-HER alloy [30].
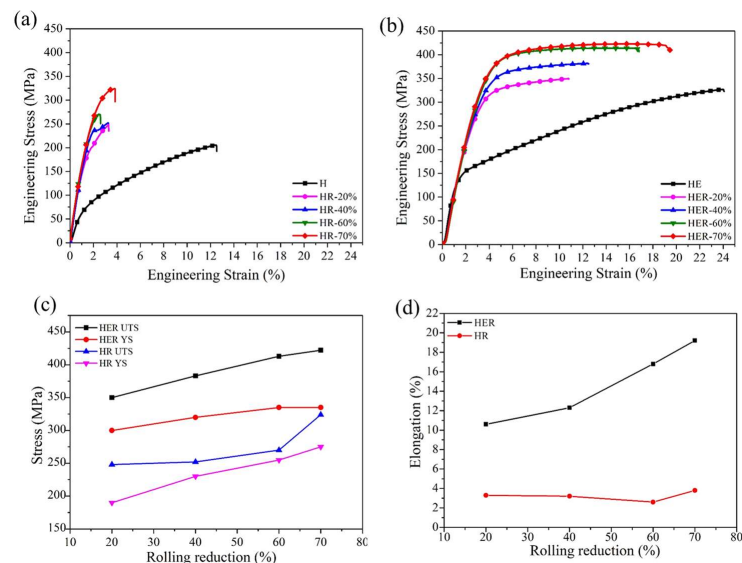

Figure 4. (**a**,**b**) Typical stress–strain curves of the AZ91 alloys at different processing states, and (**c**,**d**) tensile property comparisons of the HR and HER alloys presented in (**a**,**b**) [30].

4. Discussion

The results presented show that rolling reduction significantly influences the microstructure and mechanical properties of the H and HE AZ91 alloys. Twinning is the main deformation mechanism during further rolling of the H alloys. As the rolling reduction increased, twinning occurred more evidently and the mechanical properties of the HR alloys were slightly improved. As for the HE alloys, the microstructure was greatly changed from a homogenous type to a bimodal type when the rolling reduction increased from 20% to 70%, contributing to significant enhancements of the mechanical properties.

Figure 5 presents the schematic diagram of the microstructure evolution of AZ91 alloys processed by ECAP and SPR with varied rolling reduction. As demonstrated in Figure 5a, the HE alloy had a homogenous fine grain structure, and a large number of second phases were around the grain boundaries. After preheating, the grains grew up and the second phase dissolved into the matrix, as illustrated in Figure 5b. When the alloy was rolled with lower rolling reduction of 20% and 40%, twinning occurred preferentially, as shown in Figure 5c,d. When the rolling reduction was increased to 60% and 70%, a bimodal grain structure was formed, where coarse grains were encased in fine ones, as presented in Figure 5e. These results show that the rolling reduction plays an important part in the formation of a bimodal structure. As has been discussed in our previous work [30], the formation of a bimodal structure is mainly attributed to dynamic recrystallization, second-phase deposition, and grain growth. The fine grains are mainly caused by dynamic recrystallization (DRX) and second-phase pinning. When the rolling reduction is low, the driving force for recrystallization is insufficient, and twinning is the main deformation mechanism. When the rolling reduction is high, the large strain is difficult to disperse evenly among the original grains. There are more strains concentrated near the grain boundaries, and high-density dislocations accumulate nearby, facilitating DRX. The fine grains produced by ECAP provide a large number of grain boundaries, providing rich nucleation locations for dynamic recrystallization and second-phase precipitation, generating a high proportion of fine grains with tiny β-$Mg_{17}Al_{12}$ particles near the grain boundaries.
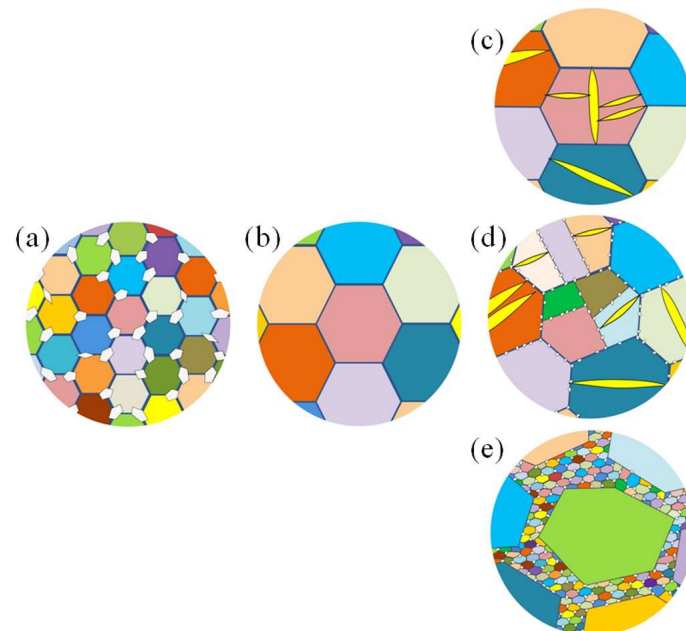

Figure 5. Schematic diagram of the microstructure evolution of AZ91 alloys processed by ECAP and SPR with varied rolling reductions: (**a**) HE, (**b**) heated HE alloy, (**c**) HER-20%, (**d**) HER-40%, (**e**) HER-60% & 70%.

Grain growth related to grain boundary migrations is still the main formation mechanism of the coarse grains. As the alloys were preheated at a high temperature, the grains

grew up quickly. However, when the effect of rolling reduction on the grain-size statistics in this study are carefully compared, it is found that the coarse grain size of the alloys rolled with higher rolling reductions has a wider range than that of the alloys rolled with lower rolling reduction. This implies that grain deformation caused by rolling also has a non-negligible influence on the formation of large grains. It is easily imagined that when the alloy is rolled, the rolling plane will stretch, while the normal and transverse planes (which are perpendicular to the rolling plane) will be compressed. As all the grains are three-dimensional, the area of the grain plane parallel to the rolling plane will expand. When the rolling reduction is low, the deformation is mild and evenly dispersed, and the grain growth is the main reason for the formation of coarse grains. This is why the grain structure of the 20%-HER alloys is very close to that of the heated HE alloys. When the rolling reduction is high, the high strain is difficult to disperse evenly within the original grains, and so grain growth and inhomogeneous deformation concurrently prompt the formation of coarse grains with a wide range of grain-size distributions.

It can be concluded that rolling reduction significantly influences the microstructures of alloys processed by ECAP and SPR. The fine grain structure provided by ECAP and the driving force from the high reduction rolling with high-temperature preheating, is responsible for the distinct bimodal microstructure. Therefore, a typical bimodal microstructure comprising coarse and fine grains is obtained in an alloy after SPR with rolling reduction of 70%. The fine grains can provide grain boundary strengthening and enhanced strength, while the coarse grains enable strain hardening and hence improve ductility, contributing to significant strength and ductility synergy in this alloy.

5. Conclusions

In this study, pre-homogenized AZ91 alloys and RD-ECAP-processed AZ91 alloys were subjected to SPR with varied rolling reductions. The effects of rolling reduction on the microstructures and mechanical properties of these alloys were investigated. The HR alloys exhibited coarse microstructures where twinning was the main deformation structure at lower rolling reductions, while twinning and narrow deformation bands were observed at higher rolling reductions. The mechanical properties of the HR alloys were poor; the UTSs were under 330 MPa and the strains were less than 5%. The HER alloys possessed finer microstructures and superior mechanical properties as compared to the HR alloys. Rolling reduction significantly influenced the microstructures of the HER alloys. The microstructures of the HER alloys were homogenous at lower rolling reductions and turned into a bimodal type at higher rolling reductions. The strength and ductility of the HER alloys were gradually improved with the increase of the rolling reduction. At the rolling reduction of 70%, excellent comprehensive mechanical properties (an ultimate strength of ~420 MPa, a yield strength of ~335 MPa, and an elongation of ~19%) were achieved in the alloy and are attributed to its bimodal structure.

Author Contributions: Conceptualization, A.M.; methodology, J.J. and Y.J.; software, J.Z.; resources, Q.X.; validation, Q.X. and Y.L.; investigation, Y.L.; formal analysis, H.L.; data curation, Y.L.; writing—original draft preparation, Y.L.; visualization, Q.X.; supervision, Y.J.; project administration, Q.X. and Y.L.; funding acquisition, A.M., Q.X., J.Z., and Y.S.; writing—review and editing, Q.X. and H.L. All authors have read and agreed to the published version of the manuscript.

Data Availability Statement: The authors confirm that the data supporting the findings of this study are available within the article.

Conflicts of Interest: The authors declare no conflict of interest.

References

1. Jayasathyakawin, S.; Ravichandran, M.; Baskar, N.; Chairman, C.A.; Balasundaram, R. Mechanical properties and applications of Magnesium alloy—Review. *Mater. Today Proc.* **2020**, *27*, 909–913. [CrossRef]
2. Joost, W.J.; Krajewski, P.E. Towards magnesium alloys for high-volume automotive applications. *Scr. Mater.* **2017**, *128*, 107–112. [CrossRef]
3. Song, J.; She, J.; Chen, D.; Pan, F. Latest research advances on magnesium and magnesium alloys worldwide. *J. Magnes. Alloy.* **2020**, *8*, 1–41. [CrossRef]
4. Wang, X.J.; Xu, D.K.; Wu, R.Z.; Chen, X.B.; Peng, Q.M.; Jin, L.; Xin, Y.C.; Zhang, Z.Q.; Liu, Y.; Chen, X.H.; et al. What is going on in magnesium alloys. *J. Mater. Sci. Technol.* **2018**, *34*, 245–247. [CrossRef]
5. Honeycombe, R. *The Plastic Deformation of Metals*; Edwaed Arnold Publishing: London, UK, 1984.
6. Nakata, T.; Xu, C.; Ohashi, H.; Yoshida, Y.; Yoshida, K.; Kamado, S. New Mg–Al based alloy sheet with good room-temperature stretch formability and tensile properties. *Scr. Mater.* **2020**, *180*, 16–22. [CrossRef]
7. Zhu, B.; Liu, X.; Xie, C.; Su, J.; Guo, P.; Tang, C.; Liu, W. Unveiling the underlying mechanism of forming edge cracks upon high strain-rate rolling of magnesium alloy. *J. Mater. Sci. Technol.* **2020**, *15*, 59–65. [CrossRef]
8. Zhou, M.; Huang, X.; Morisada, Y.; Fujii, H.; Chino, Y. Effects of Ca and Sr additions on microstructure, mechanical properties, and ignition temperature of hot-rolled Mg–Zn alloy. *Mater. Sci. Eng. A* **2020**, *769*, 138474. [CrossRef]
9. Ko, Y.G.; Hamad, K. Structural features and mechanical properties of AZ31 Mg alloy warm-deformed by differential speed rolling. *J. Alloys Compd.* **2018**, *744*, 96–103. [CrossRef]
10. Kim, Y.S.; Kim, W.J. Microstructure and superplasticity of the as-cast Mg–9Al–1Zn magnesium alloy after high-ratio differential speed rolling. *Mater. Sci. Eng. A* **2016**, *677*, 332–339. [CrossRef]
11. Song, D.; Tao, Z.; Tu, J.; Shi, L.; Song, B.; Hu, L.; Yang, M.; Chen, Q.; Lu, L. Improved stretch formability of AZ31 sheet via texture control by introducing a continuous bending channel into equal channel angular rolling. *J. Mater. Process. Technol.* **2018**, *259*, 380–386. [CrossRef]
12. Tu, J.; Zhou, T.; Liu, L.; Shi, L.; Hu, L.; Song, D.H.; Song, B.; Yang, M.B.; Chen, Q.; Pan, F.S. Effect of rolling speeds on texture modification and mechanical properties of the AZ31 sheet by a combination of equal channel angular rolling and continuous bending at high temperature. *J. Alloys Compd.* **2018**, *768*, 598–607. [CrossRef]
13. Fatemeh, G.; Roohollah, J. Asymmetric cross rolling (ACR): A novel technique for enhancement of Goss/Brass texture ratio in Al-Cu-Mg alloy. *Mater. Charact.* **2018**, *142*, 352–364.
14. Tolouie, E.; Jamaati, R. Effect of β–Mg$_{17}$Al$_{12}$ phase on microstructure, texture and mechanical properties of AZ91 alloy processed by asymmetric hot rolling. *Mater. Sci. Eng. A* **2018**, *738*, 81–89. [CrossRef]
15. Wang, H.Y.; Yu, Z.P.; Zhang, L.; Liu, C.G.; Zha, M.; Wang, C.; Jiang, Q.C. Achieving high strength and high ductility in magnesium alloy using hard-plate rolling (HPR) process. *Sci. Rep.* **2015**, *5*, 17100. [CrossRef] [PubMed]
16. Zha, M.; Zhang, X.H.; Zhang, H.; Yao, J.; Wang, C.; Wang, H.Y.; Feng, T.T.; Jiang, Q.C. Achieving bimodal microstructure and enhanced tensile properties of Mg–Al–1Zn alloy by tailoring deformation temperature during hard plate rolling (HPR). *J. Alloys Compd.* **2018**, *765*, 1228–1236. [CrossRef]
17. Yamashita, A.; Horita, Z.; Langdon, T.G. Improving the mechanical properties of magnesium and a magnesium alloy through severe plastic deformation. *Mater. Sci. Eng. A* **2001**, *300*, 142–147. [CrossRef]
18. Azushima, A.; Kopp, R.; Korhonen, A.; Yang, D.; Micari, F.; Lahoti, G.; Groche, P.; Yanagimoto, J.; Tsuji, N.; Rosochowski, A. Severe plastic deformation (SPD) processes for metals. *CIRP Ann. Manuf. Technol.* **2008**, *57*, 716–735. [CrossRef]
19. Valiev, R.Z.; Estrin, Y.; Horita, Z.; Langdon, T.G.; Zechetbauer, M.J.; Zhu, Y.T. Producing bulk ultrafine-grained materials by severe plastic deformation. *JOM* **2006**, *58*, 33–39. [CrossRef]
20. Valiev, R.Z.; Estrin, Y.; Horita, Z.; Langdon, T.G.; Zehetbauer, M.J.; Zhu, Y. Producing bulk ultrafine-grained materials by severe plastic deformation: Ten years later. *JOM* **2016**, *68*, 1216–1226. [CrossRef]
21. Jorge, A.M.; Prokofiev, E.; Triques, M.R.M.; Roche, V.; Botta, W.J.; Kiminami, C.S.; Raab, G.I.; Valiev, R.Z.; Langdon, T.G. Effect of cold rolling on the structure and hydrogen properties of AZ91 and AM60D magnesium alloys processed by ECAP. *Int. J. Hydrogen Energy* **2017**, *42*, 21822–21831. [CrossRef]
22. Furukawa, M.; Horita, Z.; Nemoto, M.; Langdon, T. Processing of metals by equal-channel angular pressing. *J. Mater. Sci.* **2001**, *36*, 2835–2843. [CrossRef]
23. Asselli, A.; Leiva, D.R.; Huot, J.; Kawasaki, M.; Langdon, T.G.; Botta, W.J. Effects of equal-channel angular pressing and accumulative roll-bonding on hydrogen storage properties of a commercial ZK60 magnesium alloy. *Int. J. Hydrogen Energy* **2015**, *40*, 16971–16976. [CrossRef]
24. Wang, L.; Jiang, J.; Ma, A.; Li, Y.; Song, D. A critical review of Mg-based hydrogen storage materials processed by equal channel angular pressing. *Metals* **2017**, *7*, 324. [CrossRef]
25. Krajňák, T.; Minárik, P.; Stráská, J.; Gubicza, J.; Máthis, K.; Janeček, M. Influence of equal channel angular pressing temperature on texture, microstructure and mechanical properties of extruded AX41 magnesium. *J. Alloys Compd.* **2017**, *705*, 273–282. [CrossRef]
26. Yuan, Y.; Ma, A.; Jiang, J.; Lu, F.; Jian, W.; Song, D.; Zhu, Y.T. Optimizing the strength and ductility of AZ91 Mg alloy by ECAP and subsequent aging. *Mater. Sci. Eng. A* **2013**, *588*, 329–334. [CrossRef]
27. Kim, W.J.; An, C.W.; Kim, Y.S.; Hong, S.I. Mechanical properties and microstructures of an AZ61 Mg Alloy produced by equal channel angular pressing. *Scr. Mater.* **2002**, *47*, 39–44. [CrossRef]

28. Lu, F.; Ma, A.; Jiang, J.; Chen, J.; Song, D.; Yuan, Y.; Chen, J.; Yang, D. Enhanced mechanical properties and rolling formability of fine-grained Mg–Gd–Zn–Zr alloy produced by equal-channel angular pressing. *J. Alloys Compd.* **2015**, *643*, 28–33. [CrossRef]

29. Yuan, Y.; Ma, A.; Gou, X.; Jiang, J.; Lu, F.; Song, D.; Zhu, Y. Superior mechanical properties of ZK60 mg alloy processed by equal channel angular pressing and rolling. *Mater. Sci. Eng. A* **2015**, *630*, 45–50. [CrossRef]

30. Li, Y.; Jiang, Y.; Xu, Q.; Ma, A.; Jiang, J.; Liu, H.; Yuan, Y.; Qiu, C. Achieving single-pass high-reduction rolling and enhanced mechanical properties of AZ91 alloy by RD-ECAP pre-processing. *Mater. Sci. Eng. A* **2021**, *804*, 140717. [CrossRef]

31. Xu, Q.; Ma, A.; Saleh, B.; Fathi, R.; Li, Y.; Jiang, J.; Ni, C. Dry sliding wear behavior of AZ91 alloy processed by rotary-die equal channel angular pressing. *J. Mater. Eng. Perform.* **2020**, *29*, 3961–3973. [CrossRef]

32. Zhu, Y.T.; Wu, X.L. Heterostructured materials. *Prog. Mater. Sci.* **2023**, *131*, 101019. [CrossRef]

33. Li, Y.K.; Zha, M.; Jia, H.L.; Wang, S.Q.; Zhang, H.M.; Ma, X.; Tian, T.; Ma, P.K.; Wang, H.Y. Tailoring bimodal grain structure of Mg-9Al-1Zn alloy for strength-ductility synergy: Co-regulating effect from coarse Al_2Y and submicron $Mg_{17}Al_{12}$ particles. *J. Magnes. Alloy.* **2021**, *9*, 1556–1566. [CrossRef]